

AD-A086 489

PHOENIX CORP MCLEAN VA

F/G 8/5

GEOPHYSICAL APPLICATIONS OF MOVING-BASE GRAVITY GRADIOMETRY. (U)

APR 80 R D BROWN

N00014-79-C-0409

NL

UNCLASSIFIED

1 of 1
AD
A00864-8

END
DATE
FILMED
8-80
DTIC

LEVEL #
PHOENIX CORPORATION

1700 OLD MEADOW ROAD, McLEAN, VIRGINIA 22102
(703) 790-1450 • TWX 710-833-0323

(12)
B.S.



Handwritten: JEE 14730

Geophysical Applications of
Moving Base Gravity Gradiometry

SDTIC
ELECTE
JUL 7 1980
SA

DISTRIBUTION STATEMENT A

Approved for public release;
Distribution Unlimited

80 4 15 009

ADA 086489

DDC FILE COPY

CONTENTS

	<u>Page</u>
Abstract	1
Gravity Gradient Measurements	3
Gravity Gradients	3
Early Measurement Techniques	4
Differential Curvature	6
Attenuation with Distance	7
Moving-Base Gravity Gradiometers	16
Crossed-Arm MBGG	16
Floating Dumbell MBGG	18
Rotating Accelerometer MBGG	19
Superconducting SQUID MBGG	21
Gravity Gradient Signatures of Geophysical Structures.	23
Sphere	23
Horizontal Cylinder	25
Vertical Fault	28
Seamount	28
Typical Gradient Magnitudes	30
Significant Parameters	33
Engineering and Operational Parameters.	33
Physical Parameters	35
Conclusions and Recommendations	38
References	39

Accession For	
NTIS GRA&I	<input checked="" type="checkbox"/>
DDC TAB	<input type="checkbox"/>
Unannounced	<input type="checkbox"/>
Justification	<input type="checkbox"/>
<i>Added on file</i>	
By _____	
Distribution _____	
Availability Codes	
Dist.	Announced/or special
<i>A</i>	

FIGURES

<u>FIGURE NO.</u>		<u>Page</u>
1	Eötvös Torsion Balance	5
2	Comparison of gravity profiles for two different structures: Vertical fault at 3 km depth; and stratigraphic trap at 1 km depth	12
3	Comparison of horizontal gravity-gradient profiles for two different structures: Vertical fault at 3 km depth; and stratigraphic trap at 1 km depth . . .	13
4	Crossed-Arm MBGG	17
5	Floating Dumbell MBGG	18
6	Rotating Accelerometer MBGG	20
7	Superconducting SQUID Gravity Gradiometer	21
8	Horizontal Gravity Gradient of a Buried Sphere for Different Measurement Altitudes	24
9	Attenuation of Horizontal Gravity Gradient of a Buried Sphere as a Function of Altitude and Depth . .	26
10	Horizontal Gravity Gradient of a Buried Infinite Horizontal Cylinder for Different Altitudes	27
11	Gravity Gradients U_{zx} of Seamounts	29
12	Gravity Gradients, U_{zx} , of Seamount Flank Crossings .	31

TABLES

<u>Table No.</u>		<u>Page</u>
1	Gravity Gradients of Geometric Bodies	8
2	Typical Marine Gravity Gradients	15
3	Marine Gravity Gradient Parameters	32
4	Significant Engineering and Operational Parameters for Moving-Base Gravity Gradiometry	34
5	Significant Physical Parameters of Moving Base Gravity Gradiometry	36

ABSTRACT

✓
The current state-of-the-art in gravity gradiometer development for moving platforms is more than adequate for geophysical survey application. An examination of the gravity gradients of several types of geological features shows that an aircraft mounted instrument with 10 Eötvös unit sensitivity and 10 second response time will be sufficient to measure geological anomalies with scale lengths as small as 5 km. Instruments under development at two different laboratories presently have better than 10 Eötvös sensitivity at 10 seconds integration time. Within 3 to 5 years, these instruments could be used in geophysical surveys.

However, research must be performed in the processing of gravity gradiometer data for geophysical parameter recovery to take full advantage of the information content of this data. Gravity gradiometry can yield much sharper definition of the shape, size, and depth of geological structures than can gravity data, because of the more rapid attenuation of the gradients with distance. This is analogous to the sharper focus and narrowed field of view provided by telescopic optics compared to the naked eye. Most of the published work on processing of gravity gradient data ignores the wealth of information contained in the gradients and recommends simply integrating a single gradient component to obtain gravity or deflection of the vertical along the survey track. These quantities are then averaged to form area mean gravity anomalies or spherical harmonic coefficients. This is sufficient for a description of the long wavelength components of the gravity field but is of little help in studying the very short wavelength features of the gravity field. For this reason, it is recommended that alternative techniques be investigated in processing the gradient data. Such techniques might include matching of signatures of gradients calculated from a suite of physical models of typical geological structures, or a least squares parameter estimation for a detailed geophysical model. In either case, it is essential that the gradiometer data from a given survey represent a range of distances from the observed structures. Only by observing the attenuation of the gradiometer signal with distance can the shape, size, and depth of the feature be resolved. This mandates the use of an aircraft as the moving base survey platform for the gradiometer: a choice which entails significant

engineering work to minimize the effect of this rather severe linear vibration and acceleration environment on the gradiometer instrument.

GRAVITY GRADIENT MEASUREMENTS

The measurements of gravity gradients have contributed significantly to exploration geophysics, particularly as an aid in gravity interpretation for locating salt domes and other oil trapping structures. But these measurements required laborious field operations with precise gravity meters or torsion balances. Recently, however, the development of very sensitive moving platform gravity gradiometers promises the possibility of rapid global high-resolution surveys of gravity gradients. In the following sections, the historical background of gravity gradient measurements is reviewed, the state-of-the-art of the new instruments is summarized and the significant parameters for a gravity survey using the new instruments are discussed.

Gravity Gradients

The gravity gradients are simply spatial derivatives of the scalar acceleration of gravity. If we define gravity \bar{g} as the gradient of the scalar geopotential u ,

$$\bar{g} = -\nabla u = -U_x \hat{i} - U_y \hat{j} - U_z \hat{k} \quad (1)$$

then the gravity gradients are given by the three directional derivatives of each of the three components of \bar{g} . Thus in local cartesian coordinates, there are nine gravity gradients. These may be written in matrix form as

$$[gg] = \begin{bmatrix} U_{xx} & U_{xy} & U_{xz} \\ U_{yx} & U_{yy} & U_{yz} \\ U_{zx} & U_{zy} & U_{zz} \end{bmatrix} \quad (2)$$

where the subscript denotes partial derivative with respect to the local horizontal and vertical coordinates, x, y, z . This form for $[gg]$ is sometimes

called the gradient tensor, although it doesn't satisfy the required contraction and transformation properties of a tensor. Because of symmetry, i.e.,

$$\left. \begin{aligned} U_{xy} &= U_{yx} \\ U_{zx} &= U_{xz} \\ U_{zy} &= U_{yz} \end{aligned} \right\} \quad (3)$$

and Laplace's equation

$$U_{xx} + U_{yy} + U_{zz} = 0 \quad (4)$$

only five of the nine gradients are independent.

Early Measurement Techniques

Gravity gradients may also be written in terms of local coordinates, where the measurement axis always lies along the local vertical, i.e., along the direction of \vec{g} . This yields only three gradients

$$U_{zx}, U_{zy}, \text{ and } U_{zz}$$

because U_x and U_y are undefined. U_{zx} and U_{zy} are called horizontal gradients and U_{zz} is called the vertical gradient. Most geophysical literature use this terminology for gravity gradients, because the gravimeters used for measurement of the gradient are usually aligned with the local vertical. For example, if the gradient is obtained using a precise gravimeter (Hammer and Anzoleaga, 1975) then readings of the total gravity acceleration along the local vertical would be taken at two locations and differenced to obtain the gradient. If the two locations were at the same elevation, but separated by a horizontal distance, then the measured gradient would be

$$U_{zx} \cong \frac{\vec{g}_2 - \vec{g}_1}{X_2 - X_1}$$

If the two locations were separated by vertical distance, then the vertical gradient would be

$$U_{zz} = \frac{\bar{g}_2 - \bar{g}_1}{z_2 - z_1} \quad (5)$$

Typical distances between stations are tens to hundreds of meters horizontally and less than 10 meters vertically.

The torsion balance has also been used to determine gravity gradients, particularly in the 1930's for oil and mineral exploration. It also is oriented in a local vertical coordinate system but, other gradients such as U_{xx} , U_{yy} , and U_{xy} may be derived from its use. It is essentially configured as a beam about 40cm long with masses of 30g or so on the ends of the bar. One or both masses may be displaced in the vertical direction for a separation of about 50cm (see Figure 1). This assembly is hung from a torsion wire and tends to

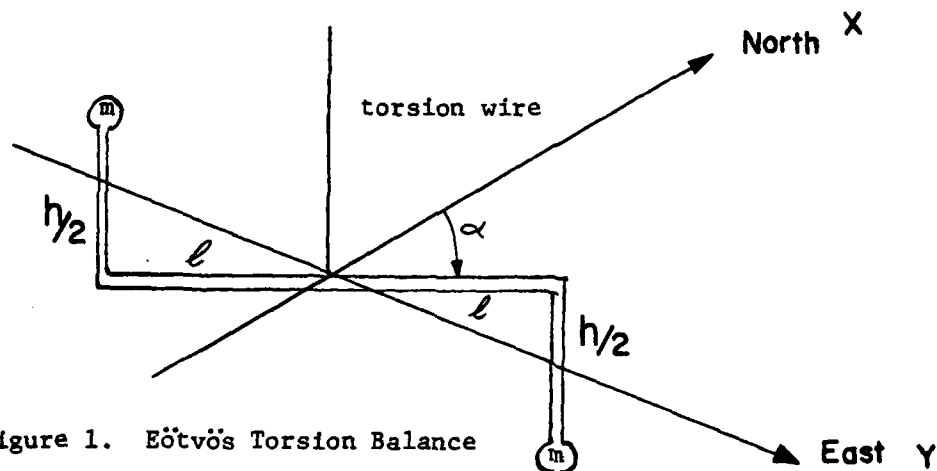


Figure 1. Eötvös Torsion Balance

rotate in a horizontal plane in response to gravity gradients. By virtue of their spatial separation, each mass senses a different value of horizontal acceleration. The measured torque is a function of U_{yy} , U_{xx} , U_{xy} , U_{xz} , U_{yz} , and the bar azimuth angle, α , measured from north. The vertical component of gravity U_z , and its gradients are not sensed because only rotation in a horizontal plane is measured. The actual equation relating the observed rotation to the gradients may be written as

$$R - R_0 = \frac{ml^2}{\tau} [(U_{yy} - U_{xx}) \sin 2\alpha + 2U_{xy} \cos 2\alpha] + \frac{mlh}{\tau} [U_{yz} \cos \alpha - U_{xz} \sin \alpha] \quad (6)$$

where τ is the torsion coefficient of the wire and R_0 is the rotation angle reading in the absence of gravity gradients. By making multiple measurements at a single location but at different azimuth angles, a solution for the 5 independent gravity gradient components and the term R_0 can be accomplished. This is tedious and painstaking work, as the balance requires about 30-60 minutes to reach equilibrium at each azimuth angle, and is very sensitive to incidental ground noise or wind currents. Heiland (1963) gives a very detailed account of the development and use of the torsion balance as a tool for geophysical explorations. Many variations of the torsion balance were constructed to minimize the measurement time at each station. Most of these variations involved additional beams inclined at various angles to the horizontal from 0° to 56° . Instruments with 2, 3, and 4 beams were developed. A four beam instrument requires observations at only 2 azimuth angles to resolve the 5 gradient components. To minimize the effect of gradients due to the proximity of the operator and field crew, some instruments were equipped with automatic photographic recorders of beam angle, and clockwork mechanisms for rotating the beams to new azimuth angles. Great care was needed in preparing the site for a torsion balance measurement. To calculate a correction for the effect of nearby topographic anomalies, the elevation of the terrain relative to the instrument location was measured out to 100 m in 8 or 16 azimuth directions, depending on the local slopes. The site was leveled with a shovel to a radius of 3 to 5 meters. There could be no ditches, embankments, or houses in the immediate vicinity. If there were trees nearby, the instrument was placed in such a way that the trees were symmetrically distributed in azimuth around the instrument. Samples of the surface soils were also taken to calculate the local density contrast. In view of these procedures, it is not surprising that the most popular measurement sites were shallow frozen lakes.

Differential Curvature

As we have seen above, the torsion balance instruments do not sense the gravity gradients directly. Rather they respond to the differential curvature of the equipotential field and gradient terms are derived from this curvature. This relation between the curvature of equipotential surfaces and gravity

gradients is useful in visualizing the gravity gradients. If all equipotential surfaces are parallel and uncurved, there can be no gravity gradients. Simple curvature, such as that created by a uniform spherical body, generates only a vertical gradient, U_{zz} , where z is directed along the radius of the sphere. For a spherical body the size of the earth, this gradient is 305.6 milligal/km or 3065 Eötvös units (E) at the surface of the earth. Of course the earth is not spherical or homogeneous, and deviations from these ideal properties cause gravity gradients which are superimposed on the normal vertical gradient. Long thin density anomalies, such as might be caused by a buried ridge, create local equipotential surfaces which have two distinct curvature axes. A torsion balance placed over such an anomaly would tend to rotate parallel to the axis of maximum curvature, i.e., normal to buried ridge axis. This is the orientation of minimum gravitational potential energy. Density anomalies of other shapes create their own distinctive curvature or gravity gradient patterns.

Attenuation with Distance

The strength of the gravity gradients also depend upon the density contrast between the anomalous body and its surroundings, and the distance from the body to the point at which the gradient is measured. This dependence on distance is much more important for measurement of gradients than for measurements of gravity. The attenuation of the gravity gradient with distance is much more rapid. Consider the gravitational effects of a spherical mass, M . The potential U of the mass is given by

$$U = \frac{GM}{r} \quad (7)$$

where G is the gravitational constant and

where r is the distance from the center of the sphere to the observation point. The gravity attraction of the sphere is

$$g = - \frac{\partial U}{\partial r} = \frac{GM}{r^2} \quad (8)$$

The vector component of gravity in the vertical direction z , is given as

$$-U_z = \frac{GMz}{r^3} \quad (9)$$

and in horizontal directions x , and y , as

$$-U_x = \frac{GMx}{r^3} \quad (10)$$

$$\text{and} \quad -U_y = \frac{GMy}{r^3} \quad (11)$$

where $r^2 = x^2 + y^2 + z^2$

Note that the gravity due to a sphere attenuates with distance as r^{-2} .

The gravity gradient may be written in general as

$$U_{uv} = \frac{\partial^2 U}{\partial u \partial v} = -GM \left[\frac{\hat{u} \cdot \hat{v}}{r^3} - \frac{3uv}{r^5} \right] \quad (12)$$

where u and v are any two coordinates x , y , or z , and \hat{u} , \hat{v} are unit vectors in the direction of u and v .

If u and v are orthogonal, then $\hat{u} \cdot \hat{v} = 0$ and

$$U_{uv} = \frac{3GMuv}{r^5}, \quad u \neq v \quad (13)$$

If u and v are the same, then $\hat{u} \cdot \hat{v} = 1$ and

$$U_{uv} = U_{uu} = -\frac{GM(r^2 - 3u^2)}{r^5}, \quad u = v \quad (14)$$

Note that the gradient for the sphere attenuates with distance as r^{-3} , much more rapidly than gravity.

For comparison of the gravity gradients of various geometric shapes and sizes, it is desirable to normalize the mathematical formulations in terms of some characteristic dimension of the body. This is easily done, as the gradient expression is free of units of length when the mass M is expressed as density times volume, V . Note that when the anomalous body of density σ_b is buried in a material of density σ_m , the effective mass creating the gradient is

$$M' = V (\sigma_b - \sigma_m) \text{ or } V (\Delta\sigma) \quad (15)$$

where $\Delta\sigma$ is the density contrast. If there is no density contrast, there is no gravity gradient. Thus, for the sphere of radius R , the non-dimensional formulations of the gradient are

$$U_{ij} = 4\pi G\Delta\sigma \left[\frac{ij}{(i^2 + j^2 + k^2)^{5/2}} \right] \quad i \neq j \quad (16)$$

$$U_{ii} = \frac{4}{3}\pi G\Delta\sigma \left[\frac{i^2 - j^2 - k^2}{(i^2 + j^2 + k^2)^{5/2}} \right] \quad (17)$$

where i, j, k may be any of the dimensionless parameters $x/R, y/R, z/R$. Normalized formulas for the gravity gradients of the sphere and other bodies are shown in Table 1. These formulas are found in many texts on geophysical methods. For the case of the vertical fault and the stratigraphic trap, the dimensionless parameters are $\frac{x}{t}$ and $\frac{z}{t}$, where t is the thickness of the anomalous slab.

The fact that the gravity gradient attenuates with distance much faster than the gravity is a distinct advantage in deducing the shape, size and depth of the body causing the anomaly. Also, the gradients tend to be strong and rapidly changing at the edges of a distributed body in contrast to the broad, smoothed out patterns of the gravity data. For example, compare the gravity and horizontal gravity gradient profiles shown in Figures 2 and 3. The gravity profiles for both the stratigraphic trap (a geophysical term for the pinch-out of one type of geological strata by another) and the vertical fault have

TABLE 1
Gravity Gradients of Geometric Bodies

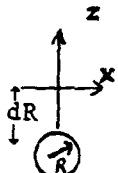
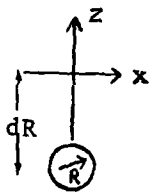
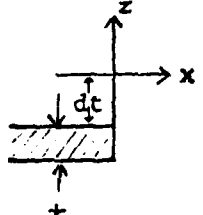
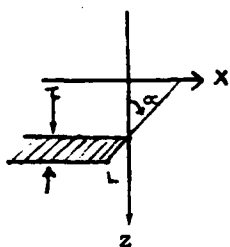
SHAPE	GRADIENT	FORMULA	SIZE	ORIENTATION
Sphere 	$U_{ik} \quad i \neq k$ U_{ii}	$-4\pi G\Delta\sigma \left[\frac{i(k+d)}{(i^2 + j^2 + (k+d)^2)^{5/2}} \right]$ $\frac{4}{3} \pi G\Delta\sigma \left[\frac{2i^2 - j^2 - (k+d)^2}{(i^2 + j^2 + (k+d)^2)^{5/2}} \right]$	Radius R $\begin{pmatrix} x = ir \\ z = kr \end{pmatrix}$	-
Long Horizontal Cylinder 	U_{ii} $U_{ik} \quad i \neq k$	$2\pi G\Delta\sigma \left[\frac{i^2 - (k+d)^2}{(i^2 + (k+d)^2)^{3/2}} \right]$ $-4\pi G\Delta\sigma \left[\frac{i(k+d)}{(i^2 + (k+d)^2)^{3/2}} \right]$	Radius R $\begin{pmatrix} x = ir \\ z = kr \end{pmatrix}$	Parallel to j axis
Vertical Fault 	U_{kk} U_{ik}	$2G\Delta\sigma \left\{ (d+1) \left[\frac{\pi}{2} + \tan^{-1} \left(\frac{i}{k+d+1} \right) \right] - d \left[\frac{\pi}{2} + \tan^{-1} \left(\frac{i}{k+d} \right) \right] \right\}$ $2G\Delta\sigma \ln \sqrt{\frac{i^2 + (k+1+d)^2}{i^2 + (k+d)^2}}$	Thickness t $\begin{pmatrix} x = it \\ z = kt \end{pmatrix}$	Parallel to j axis

TABLE 1 (Cont'd)

SHAPE	GRADIENT	FORMULA	SIZE	ORIENTATION
-------	----------	---------	------	-------------

Stratigraphic
Trap



U_{ik}	$2G\Delta\sigma \sin \alpha \left\{ \sin \alpha \ln \sqrt{\frac{(i + \tan \alpha)^2 + (k + 1)^2}{i^2 + k^2}} \right.$ $\left. + \cos \alpha \left(\tan^{-1} \left[\frac{\tan \alpha + i}{k + 1} \right] - \tan^{-1} \left[\frac{i}{k} \right] \right) \right\}$	thickness t $\begin{pmatrix} x = it \\ z = kt \end{pmatrix}$	Parallel to j axis
----------	---	--	-----------------------

U_{kk}	$2G\Delta\sigma \sin \alpha \left\{ \cos \alpha \ln \sqrt{\frac{(i + \tan \alpha)^2 + k + 1)^2}{i^2 + k^2}} \right.$ $\left. - \sin \alpha \left(\tan^{-1} \left[\frac{\tan \alpha + i}{k + 1} \right] - \tan^{-1} \left[\frac{i}{k} \right] \right) \right\}$		
----------	--	--	--

U_{ii}	$- U_{kk}$		
----------	------------	--	--

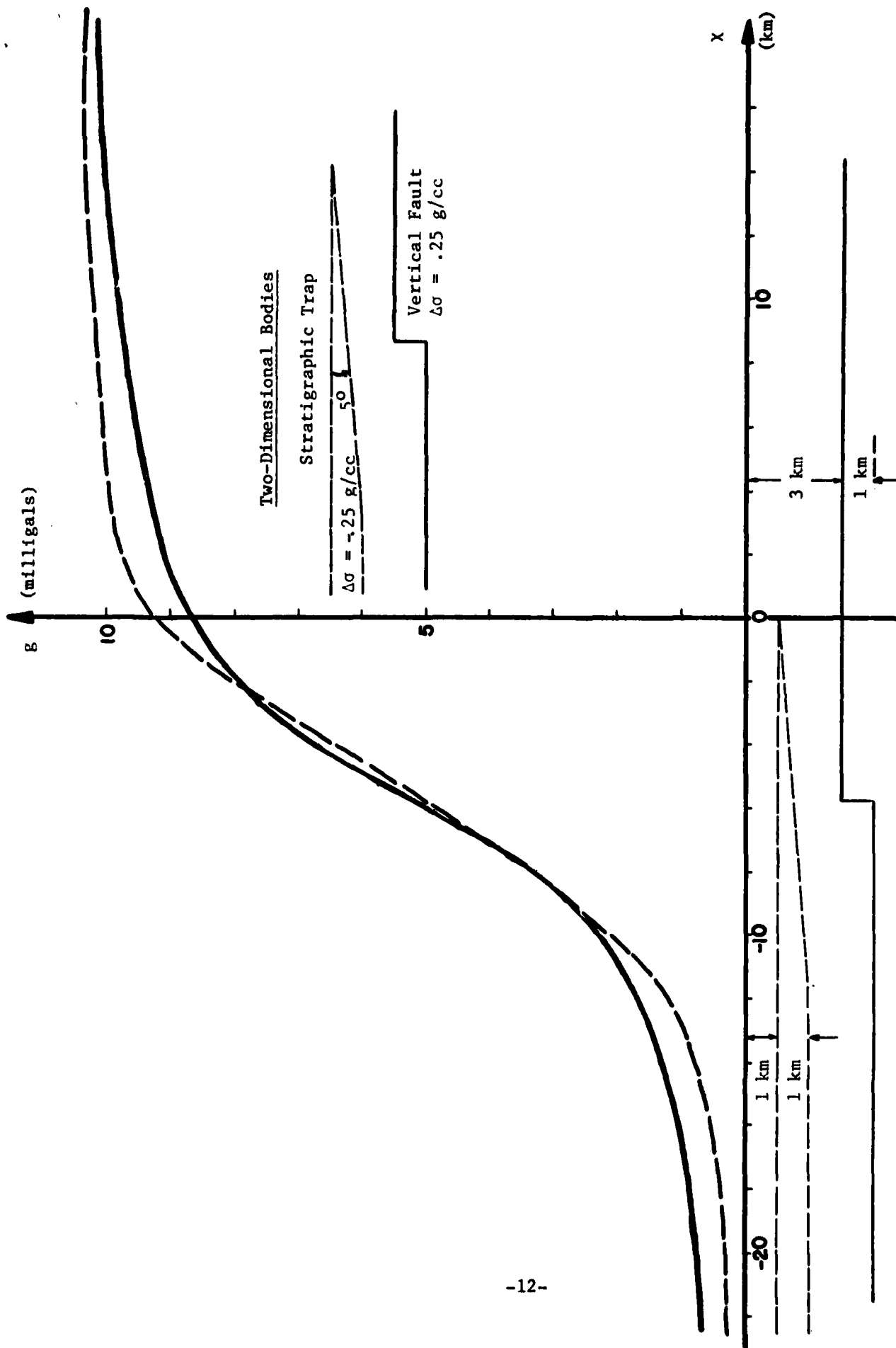


Figure 2. Comparison of gravity profiles for two different structures: Vertical fault at 3 km depth; and stratigraphic trap at 1 km depth. Note the similarity of the profiles.

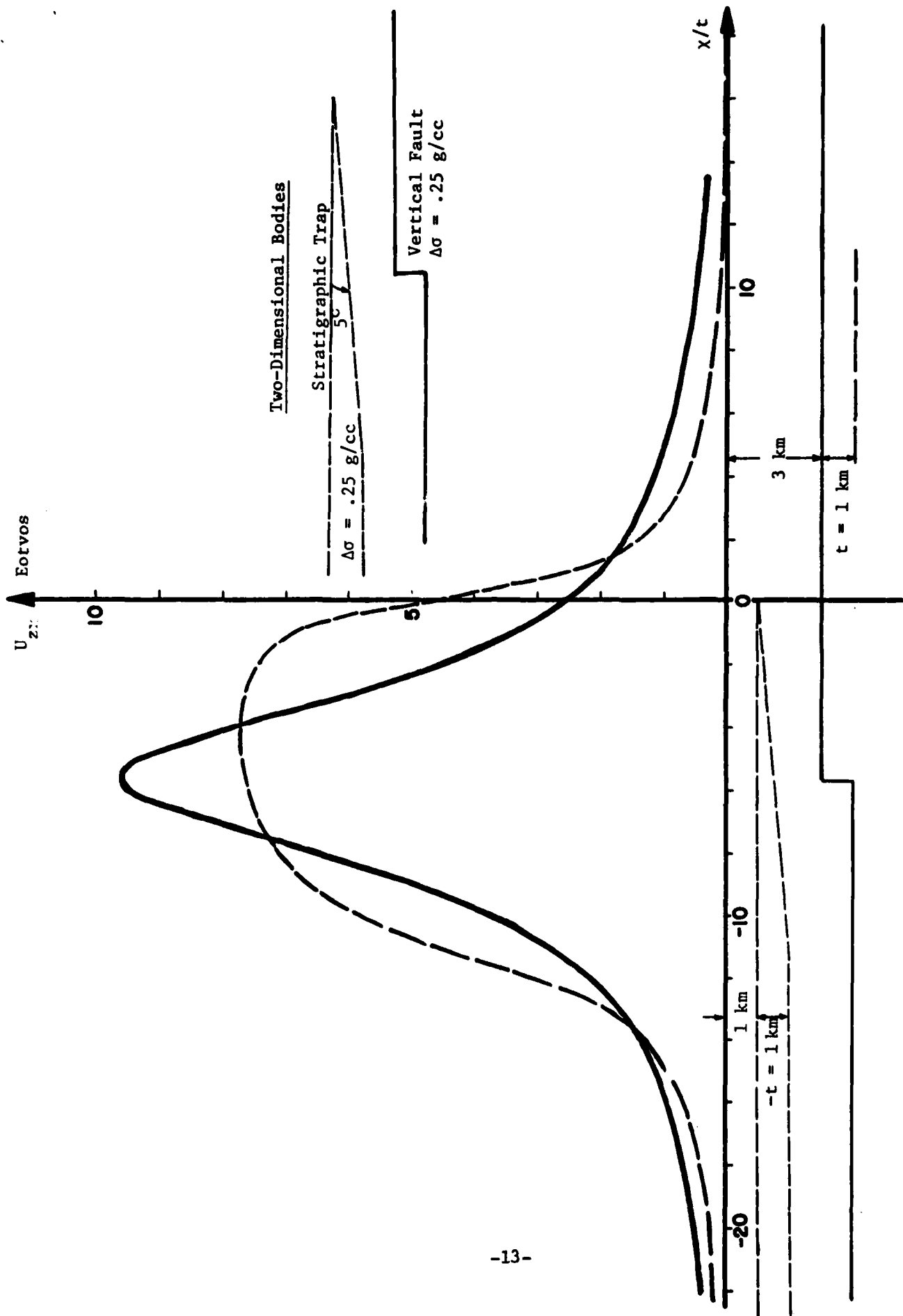


Figure 3. Comparison of horizontal gravity-gradient profiles for two different structures: Vertical fault at 3 km depth; and stratigraphic trap at 1 km depth. Note the dissimilarity of the profiles and the delineation of the edges of the structures in the gradient profile.

the same smooth shapes, despite the very different geology and shape of these structures. The depth of the vertical fault was chosen specifically so that its gravity profile would match the gravity profile of the stratigraphic trap. This demonstrates that gravity data is a relatively poor discriminant of different geological structures. In contrast, the horizontal gradient profiles of these structures shown in Figure 3 show very dissimilar shapes, and the edges of the structure are sharply defined in the gradient. There is much less likelihood of an erroneous or ambiguous identification of structure with the gradient data than there is with the gravity data. This behavior holds for other structures as well, even those which cause only a small gravity anomaly. For example, in Table 2, the salt dome, which causes a 6 mgal gravity anomaly but has well defined boundaries, has a gravity gradient of the same order of magnitude as that of an ocean trench. On the other hand, broad features with no distinct boundaries such as mid-ocean ridges, may have sizeable gravity anomalies, but low gradients.

TABLE 2

Typical Marine Gravity Gradients

<u>Feature</u>	<u>Surface Gravity (mgal)</u>	<u>Surface Gravity Gradient, U_{zx} (E)</u>
Mid-Ocean Ridge	50	1
Ocean Trench	250	50
Submarine Escarpment	100	50
Seamount	40	50
Salt Dome	6	25

MOVING-BASE GRAVITY GRADIOMETERS

The principal limitation of gravity gradient measurements made with torsion balance or gravimeter is the length of time needed to conduct a survey, even of a local area. Even though gravimeters have been operated successfully in high-speed aircraft (Nettleton, et. al., 1962), the sensitivity of the data to altitude variations and velocity changes (Eötvös effect) required careful and lengthy data processing. Meanwhile, there has arisen a need in military navigation applications for real-time estimates of gravity along the track of a moving platform.

High-performance inertial guidance systems used in these applications have a performance level where uncertainties in gravity are the largest source of navigation error (Metzger and Jircitano, 1977). Modern gravimeters are inadequate to meet this need for real-time gravity measurements because of the critical requirement for accurate altitude and velocity. Since the gravity gradient measurement is much less sensitive to these parameters than the gravity measurements, there have been a number of moving-base gravity gradiometer instruments proposed in the past decade for inertial navigation and gravity survey applications.

By integration of these gravity gradient measurements, a real-time estimate of gravity can be obtained to minimize navigation system errors. At the same time, these derived quantities of gravity and position are the essential ingredients for a gravity survey for geodetic and geophysical applications. Thus, the development of moving-base gravity gradiometers contributes to both navigation and earth science applications.

Crossed-Arm MBGG

The first moving-base gravity gradiometer (MBGG) was proposed by Forward [1962]. This instrument, and all other modern MBGG instruments, is basically a variation of the old torsion balances developed by Cavendish and Eötvös. The gravity gradient is measured as a torque on a set of proof masses separated by a short moment arm. This configuration gives a degree of independence of the instrument from accelerations of the vehicle as well as from the ambient

acceleration of gravity. The instrument developed by Forward consists of two such moment arms connected by a flexural pivot (see Figure 4) and rotated at half the torsional resonant frequency. A gradient in the gravity field in which these crossed arms are rotated will induce a flexing motion of the arms at their resonant frequency (twice the rotation frequency) while inertial effects caused by any accelerations of the proof mass mounting structure will induce motions at the rotation rate.

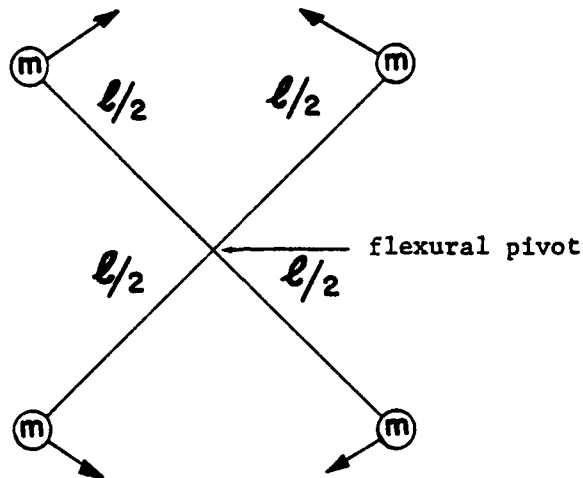


Figure 4. Crossed-Arm MBGG

By sensing the strain at the flexure, a measure of the differential torque between the moment arms can be obtained. If the torsion and rotation axis is the Z axis, then the differential torque ΔT is expressed as

$$\Delta T = \frac{ml^2}{2} \left[(U_{yy} - U_{xx}) \sin 2\omega t + 2U_{xy} \cos 2\omega t \right] \quad (18)$$

where ω is the rotation rate.

Note the similarity between this equation and equation 6 for the Eötvös torsion balance.

Mounted in a spinning satellite with m of 2kg and l of 96cm, the projected sensitivity is .01E at 30 seconds integration time (Forward, 1972).

This configuration is very sensitive to linear vibration along the spin axis (Forward, 1979, personal communication) which limits its application to unmanned spacecraft environments.

Floating Dumbbell MBGG

To minimize the vibration sensitivity of high-performance gradiometers mounted in moving vehicles, Trageser (1970) conceived of using proof masses that were floated in a viscous fluid (see Figure 5). This is essentially an Eötvös torsion balance with zero restoring torque and no means of direct transmission of vibration from the vehicle to the proof masses. In practical

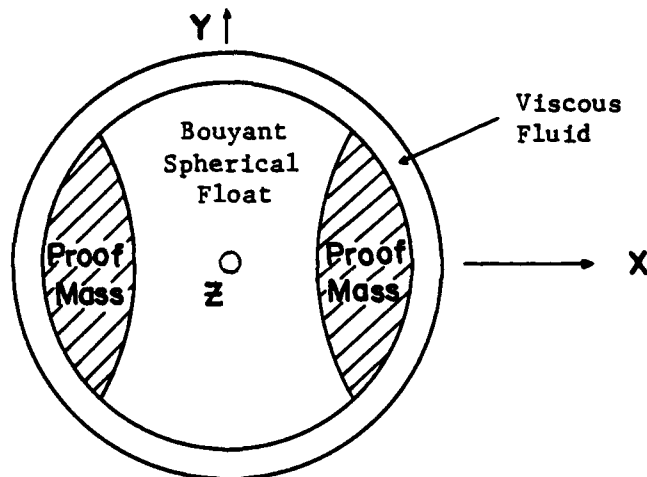


Figure 5. Floated Dumbell MBGG

application, the dumbell is not strictly free to rotate to an orientation of minimum gravitational potential energy in the presence of a gravity gradient. Motion of the dumbell is sensed and its critial orientation is restored by a feedback loop using electrostatic torques. The torque applied by the feed-back loop is indicative of the strength of the gravity gradient. Since the float is spherical, it can rotate about more than one axis. In the case shown in Figure 5, rotation about both the Y and Z axes is permitted. The measured torques about each axis are given in terms of gravity gradients as

$$T_z = I \left[(U_{yy} - U_{xx}) \sin 2\alpha + 2U_{xy} \cos 2\alpha \right] \sin \beta$$

and

$$T_y = I \left[(U_{zz} - U_{xx}) \sin 2\beta + 2U_{xz} \cos 2\beta \right] \sin \alpha$$

where I is the largest moment of inertia of the float and α and β are the angles of the rest position of the axis of weights relative to the X and Z axes respectively. Note again the similarity of these equations to equation 6 for the Eötvös torsion balance. This type of MBGG features relative immunity to Brownian motion noise and vehicle vibration. However, it does exhibit base line shift and long term drift effects which appear not to be predictable (Trageser and Johnson, 1980). The instrument self noise at 10 seconds integration time is about $3E$ (Brown, 1980). A simulation of the recoverability of gravity from this type of MBGG in an aircraft survey at 20,000 feet, indicates an accuracy of about 8 mgal RMS (Brown, 1980). This is significantly better than was obtained with the earlier gravimeter aircraft flights, even though they were at lower altitudes and with longer integration times.

There are currently 4 instruments of this type in storage. They could be made available for use in geophysical surveys within 2 years (Trageser, 1979, personal communication).

Rotating Accelerometer MBGG

Another type of MBGG has also been developed recently which shows promise for use in aircraft geophysical surveys. This is the MBGG developed by E. Metzger at Bell Aerospace Textron. This gradiometer was developed from off-the-shelf accelerometer parts of a sensitive ship mounted gravimeter which has been in production since 1966. Mr. Metzger found that if two of these accelerometers were separated by some distance, X , then the differential gravity acceleration (or gravity gradient), U_{zx} , could be measured. Another pair, oriented at right angles to the first pair, could measure U_{zy} . And if the entire set of four accelerometers were rotated at some known rate, then the bias errors peculiar to each accelerometer could be detected and removed. This is the concept of the rotating accelerometer MBGG (Figure 6).

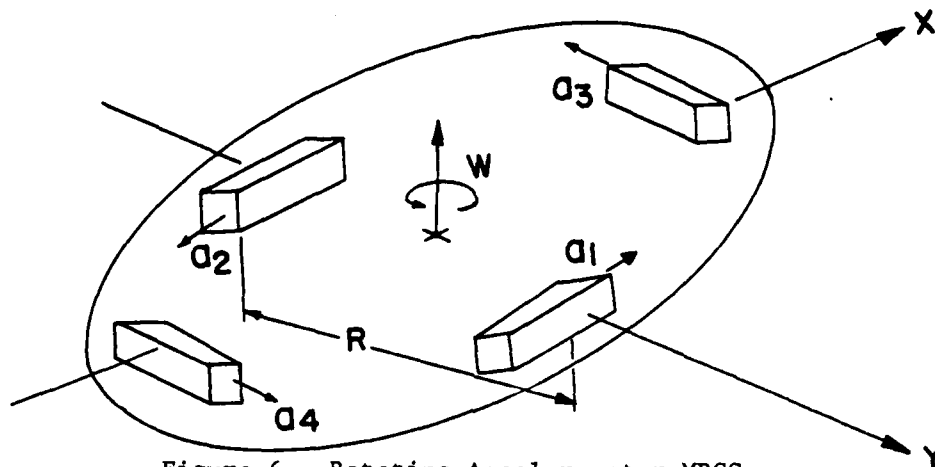


Figure 6. Rotating Accelerometer MBGG.

The output of the accelerometers is summed to reject linear acceleration perpendicular to the spin axis and angular acceleration about the spin axis. If the spin axis is vertical, the measurement equation is

$$(a_1 + a_2) - (a_3 + a_4) = 2R(U_{xx} - U_{yy}) \sin 2\omega t + 4RU_{xy} \cos 2\omega t$$

By operating two such rotating arrays with orthogonal spin axes, all 5 independent gradient components may be observed. The major engineering problem remaining to be solved with this MBGG is the problem of platform jitter caused by stiction. This refers to the irregular motion of the stable platform to which the MGBB is mounted. During periods of light or no-load, the platform gimbal bearings stick and then break loose suddenly causing high angular accelerations on the MBGG (Brown, 1980). At the present state of development, 7E sensitivity at 10 seconds integration time has been attained in static tests, and this instrument has been chosen by the Navy Special Projects Office for sea trials beginning in 1981. Simulation test of this instrument performing in the severe vibration environment of an aircraft for airborne gravity surveys show about 14 mgal RMS error in gravity recovery from an altitude of 20,000 feet (Brown, 1980).

Superconducting SQUID MBGG

There are other types of gravity gradiometer instruments which have been proposed, but which are not as far along in development as the three mentioned above. The most suitable of these for moving-base survey application is the cryogenic gravity gradiometer being developed at the University of Maryland by Prof. H. J. Paik. It makes use of superconducting currents and inductive transducer coupling to a very sensitive superconducting magnetometer called a SQUID. The circuit diagram is shown in Figure 7. By lowering the device to superconducting temperatures, Brownian motion noise is substantially reduced, as is electronic noise related to temperature.

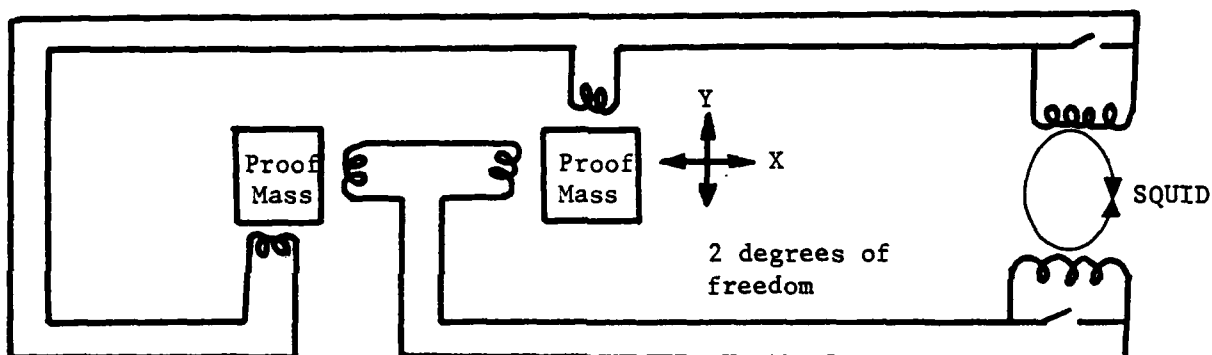


Figure 7. Superconducting SQUID Gravity Gradiometer.

By common-mode balancing, one can measure gradients U_{xx} and U_{yy} separately. Most other gradiometers measure $U_{xx} - U_{yy}$, as does the Eötvös torsion balance, because of a rigid connection of some kind between the proof masses.

The design goal of the University of Maryland gradiometer is $10^{-4} \text{ E}^2/\text{Hz}$ sensitivity. At 10 seconds integration time, this corresponds to .003E sensitivity. Such high sensitivity is needed for its proposed use in a satellite mission to map the earth's gravity field on a global basis. It is expected to be ready for a flight test on the Space Shuttle in 1984 or 1985.

Thus, in the near future, there will be several gravity gradiometer instruments which can fulfill the requirements for speed of operation and survivability in the high vibration environment of a moving vehicle. The

sensitivity of these instruments is also sufficient for recovery of important new knowledge about gravity and geophysical structure, as will be demonstrated in the next section.

GRAVITY GRADIENT SIGNATURES OF GEOPHYSICAL STRUCTURES

To investigate possible geophysical applications of moving-base gravity gradiometry, it is interesting to examine the gravity gradient signatures of common geophysical structures. By modeling common geometric structures and computing their gravity gradients, the differences in gradient signatures can be noted and the ability to discriminate between structures based on these differences can be evaluated. Performance requirements for a moving-base gravity gradiometer survey mission can also be indicated from analysis of these modeled signatures.

Some gravity gradient signatures of a sphere, a cylinder, a vertical fault, stratigraphic traps, and seamounts, will be examined at various depths and survey altitudes. This is not intended to be an exhaustive study, just a brief look to identify directions for more intense research.

Sphere

Figure 8 shows the horizontal gravity gradient signature U_{zx} of a buried sphere of radius R , and density contrast, $\Delta\sigma$, of .25 grams per cubic centimeter. The sphere is buried with the surface of the sphere just tangent to the ground surface. The attenuation of the maximum value of the gradient with altitude is shown also. The formula for the gravity gradient of the sphere is given in Table 1.

The U_{zx} signature of the sphere is typical of any finite body. The gradient signature is bipolar with the peak values occurring near the edges of the body. The peak values attenuate with altitude quite rapidly, inversely proportional to the cube of the altitude. It is interesting to note that the position of the peak value of the signature also shifts with altitude. For a sphere at depth $D=R$, the peak value occurs at $X_{\max} = R/2$ for $Z=0$. As Z increases, the position of the peak moves out away from the body center. At higher altitudes the peak value is given by

$$X_{\max} = \frac{Z+D}{2}$$

EÖTVÖS

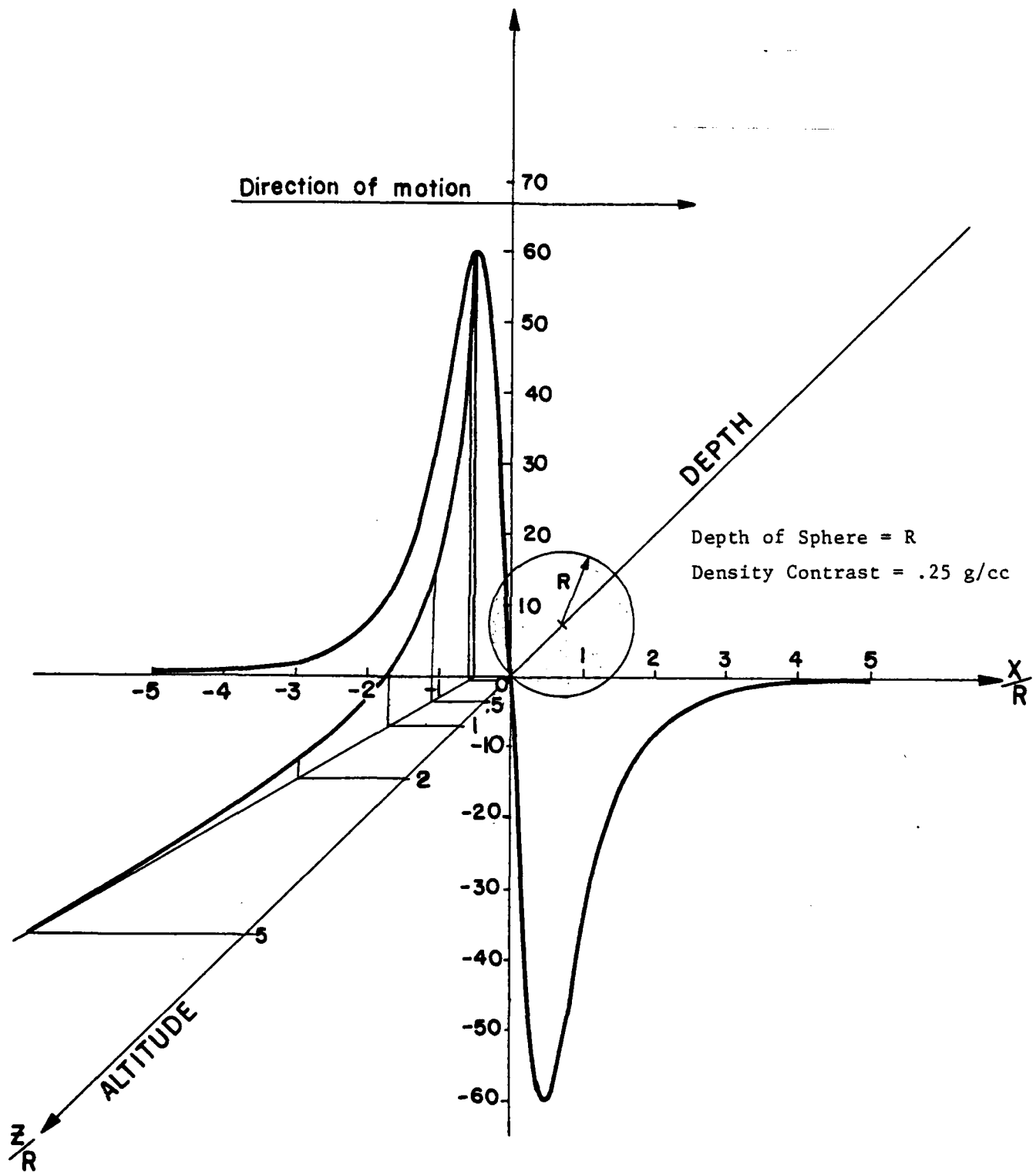


Figure 8. Horizontal Gravity Gradient of a Buried Sphere for Different Measurement Altitudes.

Thus, when $Z=5R$, the peak value occurs at $X_{\max}=3R$. As we will see in the following section this effect is a function of the shape of the body, and may prove to be a useful indicator of the shapes of unknown geophysical structures.

The value of U_{zx} for the sphere at any fixed value of X is a function of both altitude and depth as is shown in Figure 9. Note that the deeper the sphere, the less rapid is the initial attenuation rate. The final attenuation rate approaches as asymptote inversely proportional to $(Z/R)^4$. This attenuation rate and behavior with depth is unique to a sphere, and provides another possible way to determine shape from gradiometer survey data.

Horizontal Cylinder

The horizontal cylinder is typical of elongated geological structures such as ridges. It too yields a bipolar signature in U_{zx} (Figure 10), where X is the direction normal to the cylinder axis, but the tails of the signature are somewhat longer than that of the sphere. It is interesting to note by transposing coordinates in the formulas of Table 1, we can infer that the horizontal gradient of a long vertical cylinder has the same type of signature as the horizontal cylinder.

For the same radius and density contrast, the peak value of the cylinder signature is slightly higher than that of the sphere. A more striking distinction is that the rate of attenuation of the signature peak value is inversely proportional to the square of the altitude, slower than that for the sphere.

For a cylinder at depth $D=R$, the position of the peak value occurs a little further out toward the edge of the cylinder, at

$$X_{\max} = R/\sqrt{3}$$

compared to the sphere. Thus, the shift in peak value with altitude may indicate whether the buried body is a sphere or a cylinder. At a particular value of X , the signal amplitude is inversely proportional to the cube of the altitude, as opposed to the fourth power for the sphere. These distinctions show promise for the development of procedures to distinguish the shapes of bodies, as well as their depth in processing moving-base gravity gradiometer survey data.

EÖTVÖS

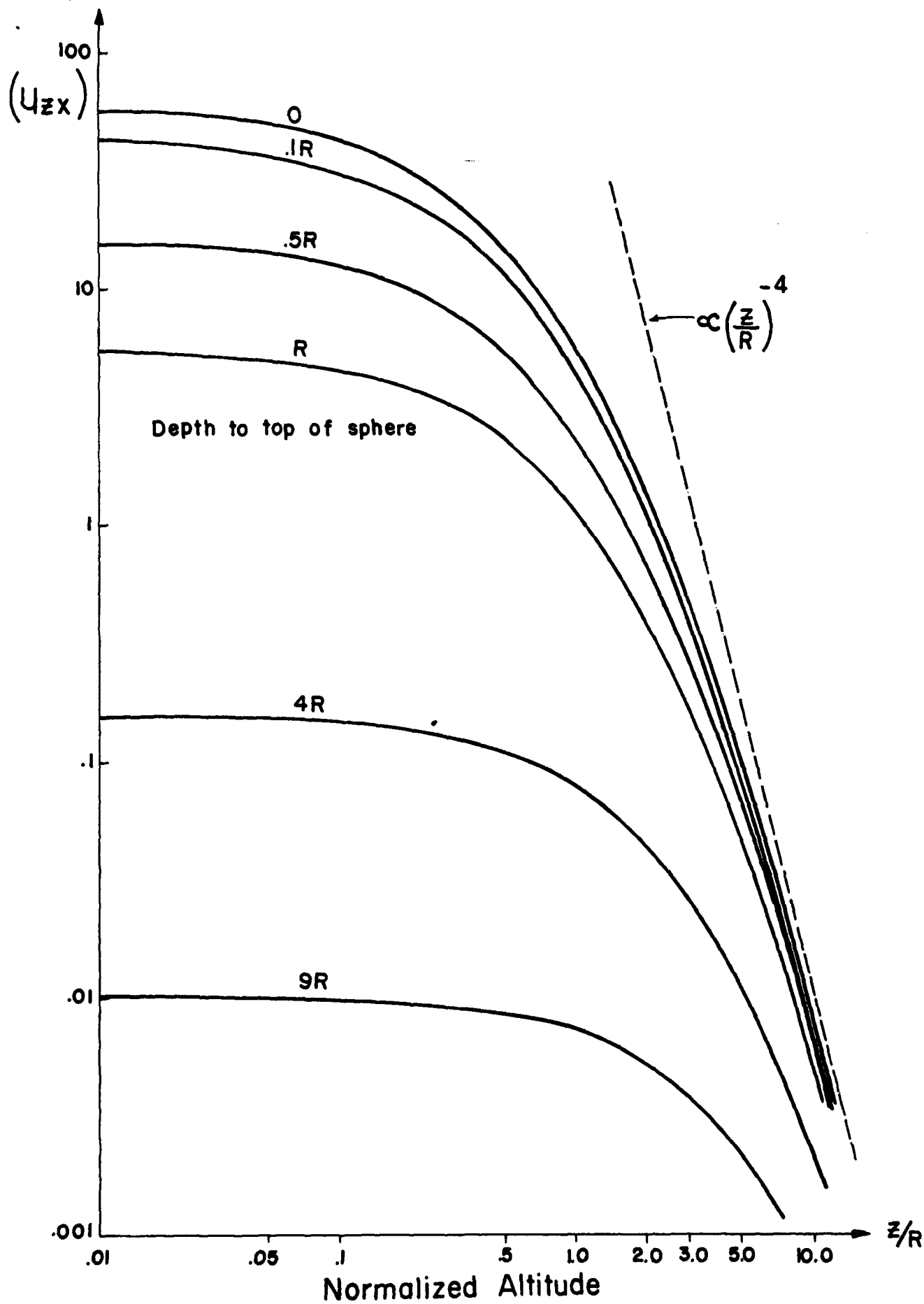


Figure 9. Attenuation of Horizontal Gravity Gradient of a Buried Sphere as a Function of Altitude Depth.

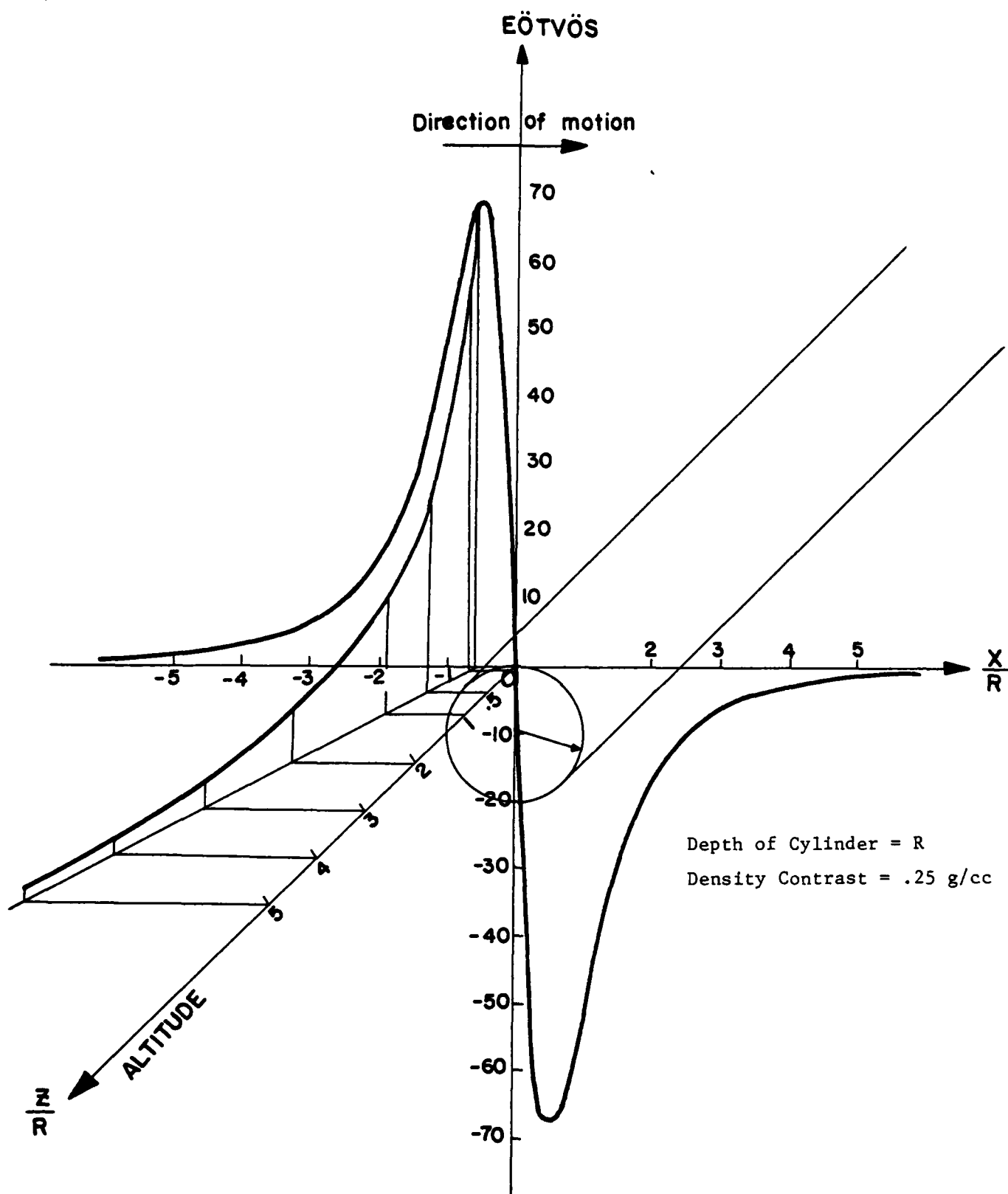


Figure 10. Horizontal Gravity Gradient of a Buried Infinite Horizontal Cylinder for Different Altitudes.

Vertical Fault

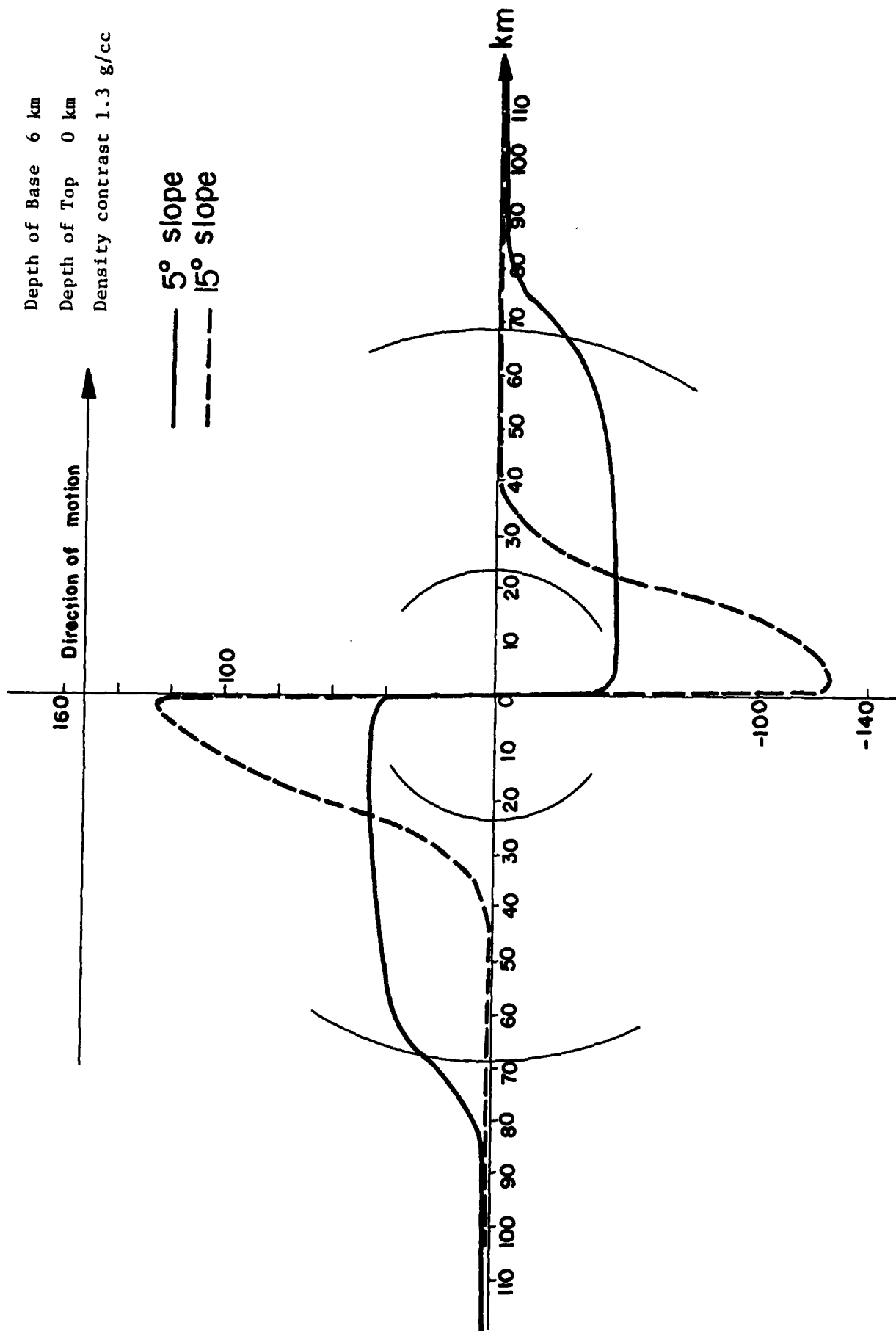
The vertical fault is typical of structures which have large extent in two horizontal dimensions, such as plateaus or grabens. The horizontal gradient of a vertical fault was shown in Figure 3, in comparison with the gradient of another similar structure, the stratigraphic trap. Note the monopolar nature of the gradient, in contrast to that of a sphere or a long cylinder. The attenuation of these signatures at any value of x with altitude is inversely proportional to altitude, a much slower rate than either the cylinder or the sphere. Thus it is not difficult to distinguish between these structures, given a gravity gradient survey at several different altitudes. It is interesting that a vertical dike, which is similar to the vertical fault but with its large dimensions in the vertical plane, would exhibit the same attenuation rate with altitude as the vertical fault, but its signature would be of a bipolar nature, like the cylinder or sphere.

There are some interesting characteristics in the shape of the horizontal gradient signature for structures such as the vertical fault. If the horizontal boundary of the structure has a vertical face, as a vertical fault, then the signature is symmetric about that edge. If it has a non-vertical slope, such as for a stratigraphic trap or an escarpment, the signature is skewed. Referring to Figure 3, the stratigraphic trap, note that the maximum positive and negative slopes in the signature correspond to the top and bottom of the horizontal layer. Hammer and Anzoleaga (1975) have carried the analysis further and find that the value of the maximum slope in the gradient is inversely proportional to the structure. Furthermore, the amplitude of the gradient is proportional to the slope angle of the horizontal boundary of the structure.

Seamount

The horizontal gravity gradient of a conical seamount has features which are similar to, yet distinct from, those of both a sphere and a stratigraphic trap. Referring to Figure 11, notice the bipolar nature of the gradient signatures, similar to the sphere. However, like the signature of the stratigraphic trap, there is a relation between the gradient amplitude and the slope

Figure 11. Gravity Gradients U_{zx} of Seamounts



of the seamount. The edges of the seamount are also evident in the gradient signature, as is the central peak. These signatures are for gravity gradient measured at the ocean surface where the seamount top is just at the surface, and are derived from gravity values calculated by Rose and Bowman (1974). The gradient attenuates inversely proportional to the cube of the distance from the seamount, like the sphere, but the shape of the signature is more like that of the stratigraphic trap. As the survey profiles move off the centroid of the seamount, and out onto the flank (Figure 12) the signatures become like that of a sphere, however.

Typical Gradient Magnitudes

Table 3 lists the magnitude of the horizontal gravity gradient, both at the surface, and at 10 km altitude for several typical marine geophysical structures. The response time of the gradiometer necessary to detect these signatures is indicated by the time signature value. This is simply the scale length of the feature divided by the typical aircraft speed of 200 m/sec. Note that very broad features such as the mid-ocean ridges have very small gradient values spread over a long period of time, and are thus susceptible to going undetected in the presence of shorter period gradients, such as that of the salt dome. Note also the difference in attenuation rate with altitude between the salt dome and the mid-ocean ridge.

Gravity Gradients, U_{zx} , of Seamount Flank Crossings

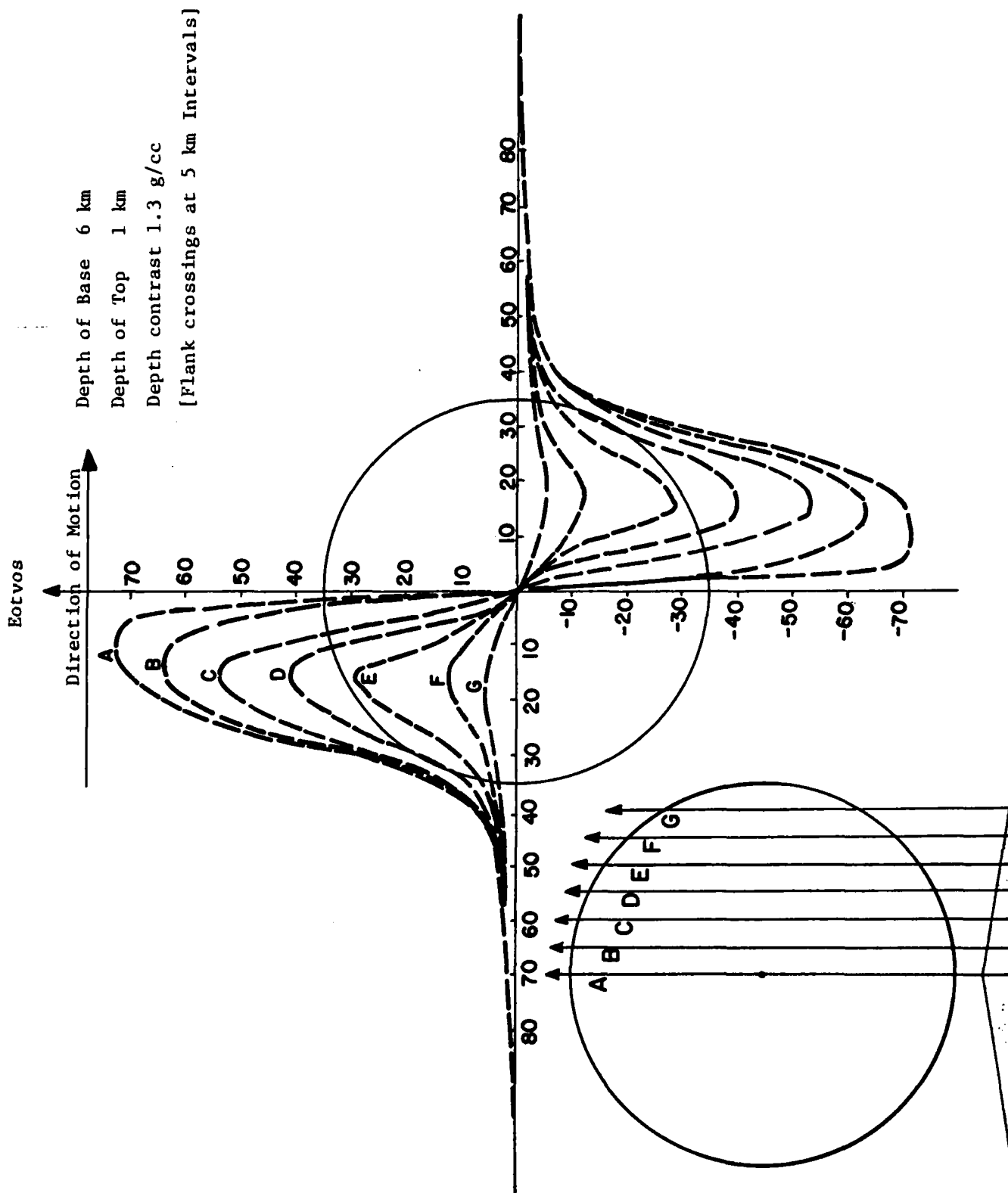


Figure 12

TABLE 3

MARINE GRAVITY GRADIENT PARAMETERS

<u>FEATURE</u>	<u>SCALE LENGTH</u>	<u>GRAVITY ANOMALY</u>	<u>SURFACE</u>	<u>10 KM ALTITUDE</u>	<u>TIME SIGNATURE AT 200 M/SEC</u>
MID-OCEAN RIDGE	600 KM	50 MGAL	1 EOTVOS	0.9 EOTVOS	3000 SECONDS
OCEAN TRENCH	50 KM	250 MGAL	50 EOTVOS	40 EOTVOS	250 SECONDS
SEAMOUNTS	70 KM	220 MGAL	50 EOTVOS	30 EOTVOS	350 SECONDS
	5 KM	40 MGAL	50 EOTVOS	5 EOTVOS	25 SECONDS
SUBMARINE ESCARPMENT	20 KM	100 MGAL	50 EOTVOS	25 EOTVOS	100 SECONDS
SALT DOMES	3 KM	6 MGAL	24 EOTVOS	0.4 EOTVOS	15 SECONDS
	50 KM	0.4 MGAL	52 EOTVOS	0.005 EOTVOS	0.3 SECONDS

SIGNIFICANT PARAMETERS

The foregoing sections have described in some detail the parameters of the gradiometer instrument and the geophysical structures which cause the gravity gradients. The purpose of this section is to identify those parameters which may be important in a geophysical survey to better describe the marine gravity field.

Engineering and Operational Parameters

Instrument response time is one of the most important of the engineering and operational parameters (Table 4) in designing a gradiometer survey. As was shown in Table 3, there is a wide range of scale lengths represented in typical marine geophysical structures. The aircraft (or other moving vehicle) speed must be chosen such that those geophysical structures which are to be measured in the survey will have a time signature which is longer than the response time of the gradiometer. Typical design response times for the MBGG described earlier are about 10 seconds. That is, the instrument averages gradient readings obtained over a 10 second time interval in order to minimize noise errors. This would be too short at 200 m/sec. for measurement of the small salt dome in Table 3.

Instrument sensitivity is another significant parameter, together with survey altitude. The sensitivity of the MBGG instruments described earlier ranges from .003 E at 10 seconds for the U. of Maryland instrument to 7E at 10 seconds for the Bell MBGG. To be detectable, the gravity gradient must have a magnitude greater than the instrument sensitivity at the altitude of the survey. Thus, the Bell instrument would miss the salt domes, the smaller seamounts, and the mid-ocean ridge at 10 km altitude, but could measure all but the mid-ocean ridge at sea level.

Attitude determination is another significant parameter, since the new generation of MBGG instruments operate without knowledge of the direction of the local vertical. With a gravimeter or torsion balance, there is only one direction to determine and that is North (x). The local vertical (z) direction is established by the equilibrium position of the torsion balance and/or levelling

TABLE 4

SIGNIFICANT ENGINEERING AND OPERATIONAL PARAMETERS
FOR MOVING BASE GRAVITY GRADIOMETRY

- INSTRUMENT RESPONSE TIME
- SPEED (MAGNITUDE AND DETERMINATION)
- INSTRUMENT SENSITIVITY
- ALTITUDE
- ATTITUDE DETERMINATION
- VIBRATION AND VEHICLE ACCELERATIONS
- POSITION DETERMINATION
- LOCAL GRADIENTS (MOTION OF INSTRUMENT GIMBALS, OBSERVERS)

bubbles on the gravimeter. The East direction (Y) is determined to be orthogonal to the North and vertical directions. The new MBGG instruments, however, can operate in any altitude, due to their multiple degrees of freedom. With the motion of the vehicle, this altitude can change from one measurement to the next. Thus it is especially important to actively determine the altitude of the MBGG measurement axes relative to the East, North, Vertical or to an inertial coordinate system during the survey.

The vibration environment of the MBGG during the survey is of critical importance. The instrument noise due to vehicle vibration can increase dramatically (by several orders of magnitude), resulting in an effective decrease in instrument sensitivity. For the Bell instrument, the sensitivity decreases by up to $1.7 \text{ E per cm/sec}^2$ of linear acceleration, at all frequencies (Brown, 1980). The degree to which the MBGG can be isolated from or made immune to the vehicle vibration enhances the measurability of small gravity gradients.

The least important of the significant parameters for MBGG survey operations is the position determination of the instrument (or vehicle) at any point in time. The accuracy of survey navigation need only be as accurate as that desired for the final product (maps, charts, etc.). Unlike gravity surveys, there is no critical need for accurate altitude for computation of gravity corrections or reference values.

Physical Parameters

Table 5 summarizes the significant physical parameters of MBGG survey applications. The importance of scale length of the feature on its detectability has already been mentioned. We have also seen how the depth, density contrast, and shape of the geophysical feature affect the magnitude and signature of the gravity gradient. This section seeks to go a step farther and indicate how these important physical parameters might be deduced from a MBGG survey.

TABLE 5

SIGNIFICANT PHYSICAL PARAMETERS
OF
MOVING BASE GRAVITY GRADIOMETRY

PARAMETER	RECOVERY TECHNIQUE	PREREQUISITES
SCALE LENGTH	MULTIPLE ALTITUDE SURVEY GRID	SHAPE, LOCATION, ORIENTATION, DEPTH, DENSITY CONTRAST
DEPTH	MODELING	SHAPE, LOCATION, ORIENTATION SCALE LENGTH, DENSITY CONTRAST
DENSITY CONTRAST	MODELING	SHAPE, LOCATION, ORIENTATION SCALE LENGTH, DEPTH
SHAPE	MULTIPLE ALTITUDE SURVEY GRID	LOCATION
ORIENTATION	PLANAR SURVEY GRID	LOCATION
LOCATION	PLANAR SURVEY GRID	NONE

If we assume an ideal case of no noise, with geometric gravitational bodies isolated within an otherwise homogeneous medium, Table 5 indicates how these physical parameters might be recovered. To locate the centroid of the body in the horizontal plane, a grid of survey lines at a constant altitude is sufficient, if the gradient magnitude is detectable at all. Once the centroid is located, the position of the maximum slopes of the signature will indicate the edges of the body, and thus its horizontal cross-section shape and orientation. Gradient measurements at several altitudes to establish the decay rate of the signal with altitude may be necessary to distinguish between the shapes of bodies at greater depths.

The scale length of the anomalous gravitational body refers to its characteristic dimension; the radius of a sphere or cylinder, the thickness of a slab or throw of a vertical fault. This parameter is aliased with the depth and the density contrast since all three affect the amplitude of the signal. The best approach to resolving this ambiguity is to assume a plausible scale length and density contrast, and then match the observed signal decay rate with altitude with that of predicted by calculation, to determine depth. This iterative process requires modeling of the bodies, knowledge of their shape, orientation and locations, and, above all, gradient measurements at multiple altitudes.

CONCLUSIONS AND RECOMMENDATIONS

Given the sensitivities of currently available MBGG, the magnitude of gradients of geophysical bodies of interest, and the possibility of measuring these gradients rapidly in an aircraft survey, we conclude that the present state of the art is sufficient for significant contributions to our knowledge of the marine gravity field. Two areas need attention, however, to make the best use of the MBGG measurements. We recommend first that the engineering problems of isolating the MBGG from the aircraft vibration and acceleration environment be studied, and the need for precise aircraft attitude control, be investigated.

Second, we recommend that a survey be conducted to establish the best methods for processing MBGG data to obtain gravity and geophysical information. As we have seen, the gradient signature, if it can be isolated and extracted from the data, contains much more information of geophysical importance than just the rate of change of gravity. Study of the signature shape can reveal the shape of the body, its size, and its depth. All this information is lost if the signature is merely integrated and averaged to produce an area mean free air gravity anomaly. More appropriate techniques might involve correlation of observed signatures with those calculated from models, or least square estimation of surface density layer elements at various depths.

REFERENCES

- Brown, R.D., 1980, "8th annual moving base gravity gradiometer review, February 5-6, 1980," U.S. Air Force Academy, Meeting Notes, Phoenix Corporation Internal Memorandum.
- Forward, R.L., 1962, "Mass detector," Hughes Research Laboratories Internal Report RL-59, March 19, 1962.
- Forward, R.L., 1972, "Geodesy with orbiting gravity gradiometers," Geophysical Monograph 15, The Use of Artificial Satellites for Geodesy, American Geophysical Union, Washington, DC.
- Hammer, S., and Anzoleaga, R., 1975, "Exploring for stratigraphic traps with gravity gradients," Geophysics, v. 40, no. 2, pp. 256-268.
- Metzger, E.H., and Jircitano, A., 1977, "Application analysis of gravity gradiometers for mapping of earth gravity anomalies derivation of the density distribution of the earth crust," Proceedings, 1st International Symposium on Inertial technology for surveying and geodesy, Ottawa, Canada, October 12-14, 1977.
- Nettleton, L.L., LaCoste, L.J.B., and Glicken, M., 1962, "Quantitative evaluation of precision of airborne gravity meter," Journal of Geophysical Research, vol. 67, no. 11, October 1962, pp. 4395-4410.
- Rose, J.C., and Bowman, B.R., 1974, "The effect of seamounts and other bottom topography on marine gravity anomalies," Proceedings of International Symposium on Applications of Marine Geodesy, Columbus, Ohio, June 3-5, 1974, pp. 381-396.
- Trageser, M.B., and Johnson, D.O., 1980, "Floated gravity gradiometer program, 1979-1980, presentation at Air Force Academy, 5 February 1980," Charles Stark Draper Laboratories Internal Report P-1045.

REPORT DOCUMENTATION PAGE		READ INSTRUCTIONS BEFORE COMPLETING FORM
1. REPORT NUMBER	2. GOVT ACCESSION NO.	3. RECIPIENT'S CATALOG NUMBER
	AD-A086 489	(rept.)
4. TITLE (and Subtitle)	5. TYPE OF REPORT & PERIOD COVERED	
Geophysical Applications of Moving-Base Gravity Gradiometry,	Interim November 1979 April 1980	
6. AUTHOR(s)	7. PERFORMING ORG. REPORT NUMBER	
R. D. Brown		
8. CONTRACT OR GRANT NUMBER(s)	9. PERFORMING ORGANIZATION NAME AND ADDRESS	
	Phoenix Corporation 1700 Meadow Road McLean, Virginia 22102	
10. PROGRAM ELEMENT, PROJECT, TASK AREA & WORK UNIT NUMBERS	11. CONTROLLING OFFICE NAME AND ADDRESS	
	Office of Naval Research Earth Physics Program 800 N. Quincy Street Arlington, Virginia 22217	
12. REPORT DATE	13. NUMBER OF PAGES	
April 1980	37	
14. MONITORING AGENCY NAME & ADDRESS (if different from Controlling Office)	15. SECURITY CLASS. (of this report)	
	Unclassified	
16. DISTRIBUTION STATEMENT (of this Report)	15a. DECLASSIFICATION/DOWNGRADING SCHEDULE	
DISTRIBUTION STATEMENT A Approved for public release; Distribution Unlimited		
17. DISTRIBUTION STATEMENT (of the abstract entered in Block 20, if different from Report)		
18. SUPPLEMENTARY NOTES		
19. KEY WORDS (Continue on reverse side if necessary and identify by block number)		
Gravity Gradient Geophysical Survey Moving-Base		
20. ABSTRACT (Continue on reverse side if necessary and identify by block number)		
The current state-of-the-art in gravity gradiometer development for moving platforms is more than adequate for geophysical survey application. An examination of the gravity gradients of several types of geological features shows that an aircraft mounted instrument with 10 Eötvös unit sensitivity and 10 second response time will be sufficient to measure geological anomalies with scale lengths as small as 5 km. Instruments under development at two different laboratories presently have less than 10 Eötvös sensitivity at 10		

409911

20.

seconds integration time. Within 3 to 5 years, these instruments could be used in geophysical survey.

However, research must be performed in the processing of gravity gradiometer data for geophysical parameter recovery to take full advantage of the information content of this data. Gravity gradiometry can yield much sharper definition of the shape, size, and depth of geological structures than can gravity data, because of the more rapid attenuation of the gradients with distance. This is analogous to the sharper focus and narrowed field of view provided by telescopic optics compared to the naked eye. Most of the published work on processing of gravity gradient data ignores the wealth of information contained in the gradients and recommends simply integrating a single gradient component to obtain gravity or deflection of the vertical along the survey track. These quantities are then averaged to form area mean gravity anomalies or spherical harmonic coefficients. This is sufficient for a description of the long wavelength components of the gravity field but is of little help in defining the very short wavelength features of the gravity field. For this reason, it is recommended that alternative techniques be investigated in processing the gradient data. Such techniques might include matching of signatures of gradients calculated from a suite of physical models of typical geological structures, or a least squares parameter estimation for a detailed geophysical model. In either case, it is essential that the gradiometer data from a given survey represent a range of distances from the observed structures. Only by observing the attenuation of the gradiometer signal with distance can the shape, size, and depth of the feature be resolved. This mandates the use of an aircraft as the moving-base survey platform for the gradiometer: a choice which entails significant engineering work to minimize the effect of this rather severe linear vibration and acceleration environment on the gradiometer instrument.

DISTRIBUTION LIST

Chief of Naval Research
Department of the Navy
800 North Quincy Street
Arlington, Virginia 22217

Code 100C1 (1)
Code 460 (1)
Code 463 (5)
Code 480 (1)

Commanding Officer
Office of Naval Research
Branch Office
666 Summer Street
Boston, Massachusetts 02210 (1)

Director
Naval Research Laboratory
Code 2627
Washington, D.C. 20375 (6)

Office of Research, Develop-
ment, Test and Evaluation
Department of the Navy
Code NOP-987J
Washington, D.C. 20350 (1)

Director
Defense Advanced Research
Projects Agency
1400 Wilson Blvd.
Arlington, Virginia 22209 (1)

Air Force Office of
Scientific Research
Department of the Air Force
Directorate of Physics(MPG)
Building 410
Bolling Air Force Base
Washington, D.C. 20332 (1)

Army Research Office
Department of the Army
Geosciences Division
Box 12211
Research Triangle Park,
North Carolina (1)

Defense Documentation Center
Building 5
Cameron Station
Alexandria, Virginia 22314 (12)

Defense Contract Administration
Services
Management Area Baltimore
300 East Joppa Road
Room 200, Hampton Plaza Bldg.
Towson, Maryland 21204 (1)